Available online at www.sciencedirect.com
SCIENCE DIRECT®
Coordination Chemistry Reviews 249 (2005) 2993–3006
COORDINATION CHEMISTRY REVIEWS
www.elsevier.com/locate/ccr

Review

Coordination and ligand exchange dynamics of solvated metal ions

B.M. Rode*, C.F. Schwenk, T.S. Hofer, B.R. Randolf

Department of Theoretical Chemistry Institute of General, Inorganic and Theoretical Chemistry, University of Innsbruck, Innrain 52a, A-6020 Innsbruck, Austria

Received 29 December 2004; accepted 30 March 2005
Available online 13 June 2005

Contents

Abstract

Recent developments in computer speed and capacity have opened the access to highly accurate molecular dynamics simulations based on quantum mechanically calculated forces for the chemically relevant region around ions in solution (QM/MM formalism). This accuracy, although still extremely consuming (30–300 days of CP time per simulation), is needed for reliable structural details and ligand exchange rates. A large number of main group and transition metal ions have been investigated by this approach, giving very detailed insight into the properties of these ions in solution and allowing to classify the ions by various characteristics. Most first-row transition metal ions have a very stable first hexa-coordinated solvation shell, whose vibrational distortions, however, strongly influence the dynamics of the second shell. The dynamical Jahn–Teller effect – shown to be a femto- and picosecond phenomenon – can strongly influence ligand coordination and exchange dynamics. A large number of ions with very labile solvation shell such as most main group ions, but also transition metal ions, e.g. Ag(I) and Hg(II), can change their coordination within the picosecond scale, leading to an almost simultaneous presence of several species hardly accessible by present experimental techniques. Among these ions, the structure breakers are of particular interest, and it could be shown that there are two types of them, one with a large and very labile first coordination shell such as Cs(I), the other characterised by a small first

* Corresponding author. Tel.: +43 5125075160; fax: +43 5125075127.
E-mail address: bernd.m.rode@uibk.ac.at (B.M. Rode).

0010-8545/$ – see front matter
doi:10.1016/j.ccr.2005.03.032

but an unusually large second solvation shell such as Au(I). Investigations of metal ions coordinated to ammonia ligands have shown that coordination to hetero-atoms can accelerate the ligand exchange reaction rates by several orders of magnitude, e.g. for Cu(II) and Ni(II). Simulations of ions in aqueous ammonia gave a very detailed picture of the complexity of species almost simultaneously present and illustrate the enormous difficulties encountered when trying to fit X-ray or neutron diffraction data for such systems. In general, ligand exchange rates situated in the picosecond range are far below the NMR scale, and as femtosecond laser pulse spectroscopy could not be applied so far to ionic solutions, accurate simulations have become a very important tool to access structure and dynamics of solvated ions. A number of video clips supplied on the Web as supporting material illustrates the processes occurring in solutions of the metal ions.

Keywords: Solvated ions; Ion complexes; Simulation; Dynamics

1. Introduction: the importance of metal ions in chemistry and biology

The importance of metal ions and their manifold applications in chemistry is undisputed, and their beneficial as well as detrimental activity in numerous essential biochemical processes is well known [1], the knowledge of their role and potency continuously increasing. Accurate details of the properties of metal ions in solution are crucial, therefore, for understanding the mechanism of their action in these processes, in particular the knowledge about the molecular structure and dynamics of ions and their complexes in solution. Consequently, solvated ions have been the subject of numerous experimental [2–4] and, more recently, also theoretical [5–8] studies, and several review papers have summarised the large number of related publications [9–11].

Many of the ions simply act in their hydrated form to maintain and modify electric and osmotic equilibria, others determine biological processes in combination with organic ligands, forming the active centre of enzymes or transport proteins. While in the first case the properties of the hydrated ion itself are the focus of interest, in the second case the influence of the coordination to other binding sites on the exchange dynamics of water or other small ligands is a matter of primary interest. Subtle differences in ion properties can dramatically change their biological role, thus making any major perturbation of the ratio of these ions a detrimental, if not lethal event (e.g. Na^+/K^+). To fully understand these effects and their regulatory mechanisms (*inter alia* ion channel function in membranes), general thermodynamic and electrochemical data are insufficient. A very accurate knowledge of the nanostructure of these ions and of their dynamical characteristics in aqueous environment is required.

Most of the experimental studies require the use of structural models for the fitting of spectroscopic observations in the process of interpretation. Therefore, the quality of the results is at best as good as the models used for this interpretation, and it will be shown in the present work that the composition of ionic solutions is in many cases much more complicated than the usual models being employed.

Another difficulty in the study of solvated metal ions is the enormous range of exchange rate constants encountered: for aquo-complexes the rates vary between 10^{-12} and $10^{12}\ s^{-1}$ [10], and most of the metal ions dominating biological systems exchange their ligands within the experimentally nearly unaccessible picosecond range, or can achieve an exchange mechanism accelerated to this range upon binding to other ligands [12–15]. Experimental rates for these ions must be considered, therefore, as rough estimates, until newer methods such as femtosecond laser pulse spectroscopy [16] can be extended to the study of solvated ion dynamics.

For these reasons, the demand for reliable theoretical methods to obtain both structural and dynamical data has always been strong. Unfortunately, simulation of liquids was (and actually still is) one of the most computer-time consuming procedures in computational chemistry, and thus the accuracy of earlier approaches was necessarily limited by the technical capability of computers and the affordable size of model systems. In the past few years, the limits of classical Monte Carlo (MC) and molecular dynamics (MD) simulations based on analytical pair and, eventually, 3-body potential functions were overcome, and introducing quantum mechanical calculations into the process of simulation has for the first time allowed to achieve the desired degree of accuracy for the treatment of solvated ions.

2. Molecular dynamics simulations as tool to investigate metal solvates

2.1. Classical simulations

Classical MC and MD simulations are being used for about half a century for the theoretical treatment of liquid systems. By employing a basic box with a sufficiently large number of atoms/ions/molecules and periodic boundary conditions, the physical state of a liquid with the experimental density is achieved, and the interactions between all species present are evaluated on the basis of empirically fitted or analytical potential functions, ab initio generated from pointwise calculations of interaction energy surfaces. Interaction functions were initially truncated to the pair term, but in particular for hydrated metal ions it was discovered quite soon that higher-order terms play an essential role, thus demanding at least 3-body corrections to these pair potential functions. Even then, classical simulations are not capable of describing more complicated phenomena such as the Jahn–Teller effect.

While classical simulations have been very helpful to get a first, general access to the molecular structure of pure liquids and electrolyte solutions, their limitations have made them today merely a helpful tool for the initial equilibration of such systems, to facilitate the performance of more accurate simulations with a good starting configuration.

2.2. Simulations based on quantum mechanics

Recognising the crucial importance of *n*-body terms for a satisfactory description of solvated ions (pair potentials even predict wrong coordination numbers [17–19], and facing the technically almost impossible task to construct higher than 3-body correction functions from ab initio calculated energy surfaces, the introduction of quantum mechanical evaluations of energies (MC) and forces (MD) remained the only feasible solution, besides attempts to achieve an average consideration of the *n*-body effects and quantum effects such as charge transfer by fitting polarisable potential functions to reflect some of the experimentally determined properties of liquids and solutions [20–22]. The latter efforts soon showed that none of these empirical potentials could cover all phenomena encountered in the liquid systems, thus leaving quantum mechanics as the only universal and nonempirical alternative.

The main problem in the use of quantum mechanical methods in the course of a simulation is the enormous computational effort associated with these calculations, boosting the required CPU time by a factor of 50–100 when using a sufficiently accurate level of theory and appropriate basis sets. Initial investigations had shown [23] that semiempirical MO methods and even single zeta basis set ab initio calculations are not capable of describing solvated ions in simulations.

An important attempt to introduce quantum mechanics into the description of solvated ions was the approach by Car and Parinello [24], in which small hydrated clusters of ion and 30–60 water molecules are simulated at density functional level of theory (DFT), usually with the relatively simple BLYP functional. However, this approach fails in most cases to produce correct coordination numbers, e.g. 5 instead of 6 for Cu(II) [25] and 6 instead of 8 for Ca(II) [26]. The use of more sophisticated hybrid density functionals such as B3LYP [27] improves this feature, but the corresponding computational effort is no more smaller than for ab initio calculations at Hartree–Fock (HF) level.

In order to avoid artificial symmetry effects and to include all solvation shells plus the effects of surrounding bulk, the basic simulation box should contain several hundred solvent molecules. To treat such a box completely by means of ab initio quantum mechanics is still far beyond any available computational capacities. The compromise leading to feasible computational requirements, but still maintaining the desired accuracy is to apply the quantum mechanical formalism to the chemically most important region of the system, and to retain the description by classical molecular mechanics for the remaining part of it. This idea, originally proposed for the treatment of larger biomolecules [28–31] has been successfully applied to solvated ions in the past decade [11] under the name of QM/MM simulations.

2.3. ab initio QM/MM simulations

In ab initio QM/MM simulations of solvated ions, the basic box is partitioned (cf. Fig. 1) into an inner region containing the ion plus 1 or 2 complete solvation shells ('QM region'), where all energies (MC) or forces (MD) are calculated at ab initio HF level, with double zeta basis sets plus polarisation functions, which has been shown to be the best compromise between accuracy and computational effort [32]. For heavier ions, the inner electrons are considered by – eventually relativistically corrected – effective core potentials (ECP). The remaining system ('MM region'), usually containing around 500 solvent molecules, is treated by classical molecular mechanics employing the same pair and 3-body potentials as in the classical simulations. The necessary size of the QM region varies with the number of solvent ligands attached to the ion and can be estimated from an initial classical simulation with pair plus 3-body potential functions.

The use of this approach requires a smoothing procedure in the transition region between QM and MM region, which allows transitions of solvent molecules without discontinuities, and the employment of a flexible solvent model in the MM region, compatible with the full flexibility of the molecules in

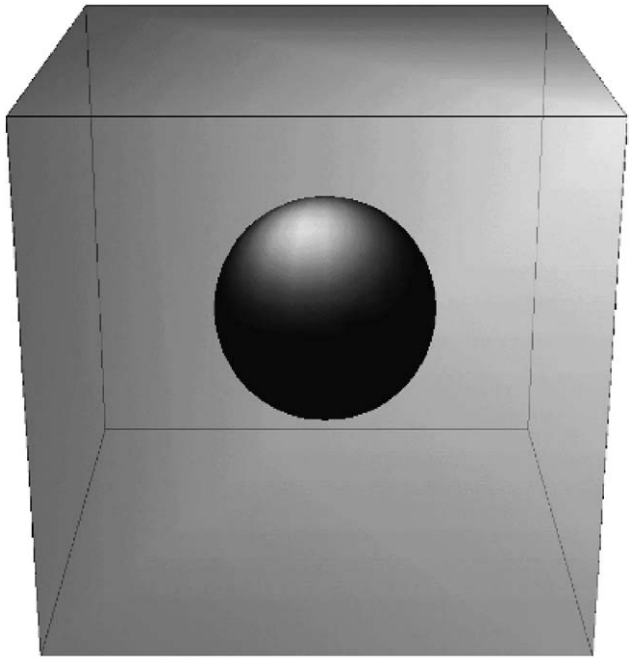

Fig. 1. Schematic drawing of the simulation box partitioned into the QM region and the rest of the simulation box treated with classical molecular mechanics.

the QM region, at least in the case of MD simulations. Such flexible model potentials always contain, in addition to the intermolecular term, an intramolecular term. This flexibility, which allows explicit hydrogen movements, also demands an appropriate short time step in the simulation, usually 0.2 fs. This requirement leads to a total amount of 50 000 steps for an MD simulation of just 10 ps, which explains the enormous computational effort of QM/MM simulations, despite of the reduction of the QM formalism to a smaller inner part of the system. One step of the simulation with the evaluation of quantum mechanically calculated forces requires a few minutes of CPU time on 4–10 processors (Intel 2400/2800 MHz) thus generating a total computation time of 30–300 days per simulation. For comparison, a classical simulation of the same systems can be performed within a few hours on a desktop computer with one processor of this type, which clearly demonstrates that most of the computational effort is dedicated to the quantum mechanical calculations. This also implies that the parallelisation of the computations has its limits in the parallelisability of the QM code (integrals, diagonalisation). With the parallel TURBOMOLE program [33–36] employed in our simulations and the aforementioned basis sets the optimal number of processors lies between 4 and 10, according to the number of ligands located in the solvation shell(s).

The MD simulation protocols of all simulations reported here were almost identical. All QM/MM MD simulations reported for ions in water have been performed for one ion immersed in 499 solvent molecules (215 molecules in the case of pure ammonia) positioned in a cubic box of the experimental density. The QM region included the full first (and eventually second) hydration sphere, and solvent molecules were allowed to enter/leave the QM region through a transition region of 0.2 Å width, ensuring a smooth transition between quantum mechanical and molecular mechanical forces. Periodic boundary conditions were applied, and long-range interactions were handled by the reaction field method. The temperature of the NVT ensembles was controlled by the Berendsen algorithm [37] with a relaxation time of 0.1 ps. For the MM part of the systems, ab initio generated pair and 3-body potential functions for ion–water interactions were used, whose details are given in the corresponding references. For water, the flexible BJH-CF2 model [38,39] was used, which allows explicit hydrogen movements, requesting thus a time step of 0.2 fs for the simulations. The preference of this water model over others is founded on the one hand on its flexibility, allowing intramolecular vibrations and relaxation processes and thus the evaluation of vibrational spectra of the ligand molecules. On the other hand, it allows a smoother transition from the QM region (where all ligands are fully flexible) to the MM region than any rigid water model would.

The pair and 3-body potential functions required for the MM region of the simulations were all constructed from the respective energy surfaces, ab initio calculated with the same basis sets thereafter used in the QM/MM MD simulations, and fitted to analytical forms of the type

$$E_{2\mathrm{bd}} = \frac{q_{\mathrm{O}} q_{\mathrm{Ion}^{n+}}}{r} + \frac{A_{\mathrm{O}}}{r^a} + \frac{B_{\mathrm{O}}}{r^b} + \frac{C_{\mathrm{O}}}{r^c} + \frac{D_{\mathrm{O}}}{r^d} + \sum_{i=1}^{2} \left(\frac{q_{\mathrm{H}} q_{\mathrm{Ion}^{2+}}}{r_i} + \frac{A_{\mathrm{H}}}{r_i^a} + \frac{B_{\mathrm{H}}}{r_i^b} + \frac{C_{\mathrm{H}}}{r_i^c} + \frac{D_{\mathrm{H}}}{r_i^d} \right) \quad (1)$$

where A, B, C and D are the final fitting parameters and a, b, c and d the exponents. q_{O} and q_{H} are the partial charges of oxygen and hydrogen, set to −0.65966 and 0.32983 [38] according to the BJH-CF2 [39,40] water model, and q_{Ion}^{n+} is the charge on the ion. The experimental gas phase geometry of H_2O was fixed during the potential surface construction with the O–H distance of 0.9601 Å and the H–O–H angle of 104.47° [41].

The 3-body correction term was constructed according to Eq. (2),

$$E_{3\mathrm{bd}}^{\mathrm{corr}} = E_{\mathrm{IonW}^i\mathrm{W}^j} - (E_{\mathrm{Ion}} + 2E_{\mathrm{W}}) - (E_{\mathrm{IonW}^i} + E_{\mathrm{IonW}^j}) - E_{\mathrm{W}^i\mathrm{W}^j} \quad (2)$$

where $E_{\mathrm{IonW}^i\mathrm{W}^j}$ is the SCF energy for $[\mathrm{Ion}(H_2O)_2]^{n+}$, E_{IonW^i} and E_{IonW^j} are the 2-body energies calculated using Eq. (1), and $E_{\mathrm{W}^i\mathrm{W}^j}$ is the interaction energy between water molecules.

To derive the 3-body potential we evaluated the energy hypersurface for H_2O–Ion^{n+}–H_2O by ab initio molecular orbital calculations at RHF/UHF level. For the geometries employed in this work almost all $E_{3\mathrm{bd}}^{\mathrm{corr}}$ values were found to be positive (repulsive) decreasing with growing ion–oxygen distances and approaching 0 kcal mol^{-1} at a distance of 6.0 Å. The resulting energies were fitted to the analytical formula:

$$E_{3\mathrm{bd}}^{\mathrm{corr}} = A\ \exp(-B\,r_{12})\ \exp(-B\,r_{13}) \times \exp(-C\,r_{23})[(r_{\mathrm{limit}} - r_{12})^2 (r_{qq\mathrm{limit}} - r_{13})^2] \quad (3)$$

with the fitting parameters A, B and C. The term in square brackets ensures that the energy for all distances above r_{limit}, i.e. 6.0 Å, vanishes. The other variables are the O–O distance, r_{23}, and the distances between the ion and the first (r_{12}) and the second (r_{13}) oxygen.

The details and parameters of all potential functions are given in the references to the specific ions cited in the following sections and tables.

Classical simulations with these potentials functions were performed to obtain suitable starting configurations for the QM/MM simulations and to obtain a measure for the necessary radius of the QM region to include the full first or first plus second solvation shell, respectively, and an eventual transition region beyond these shells.

3. Analysis of trajectories

3.1. Radial and angular distribution functions and coordination number distributions

After equilibration of the system, the history of all particle movements and their velocities are collected for the whole simulation. These trajectory files (of the size of several gigabytes for a few picoseconds of simulation) allow on the one hand to evaluate a time-averaged picture of the structures present in solution, on the other hand – with the help of a suitable software tool – a detailed presentation of the dynamical processes occurring in the time evolution, i.e. the femto- and picosecond dynamics of the system.

All types of radial distribution functions (RDF) between any pair of atoms and molecules can be evaluated separately and utilised for a very detailed analysis of the structural features of a liquid or solution. This separate evaluation is one of the main advantages of simulations, as it can be achieved only to a limited extent by experimental techniques, e.g. by isotope substitution in neutron diffraction spectroscopy, NDIS [4]. In addition to radial distributions, angular distribution functions (ADF) complement the structural details of solvate and surrounding solvent. Coordination numbers varying in time can be analysed in the form of coordination number distributions (CND), which reflect the percentual occurrence of the various ion complexes in solution, and the structure of these species can again be subjected to separate geometry analyses, thus surpassing by far any present spectroscopic capabilities.

3.2. Dynamical data: spectra, exchange rates and mean residence times

The main advantage of MD simulations compared to the MC technique is the possibility to obtain time-dependent data and thus a detailed picture of the 'real time' dynamics in a liquid system. From the velocity autocorrelation functions (VACF) rotational and vibrational spectra can be obtained by Fourier transformation [42,43], from RDFs one can obtain ligand exchange rate constants [44], and with a suitable algorithm [45] mean residence times (MRT) of ligands in a given coordination sphere can be determined from the trajectories. The latter, socalled 'dirct' method accounts all exchange events in the course of a simulation with a duration of $t > t^*$. The mean residence time of a ligand is then calculated as:

$$\tau = \frac{t_{\mathrm{sim}} \cdot \mathrm{CN_{av}}}{N_{\mathrm{ex}}} \tag{4}$$

where t_{sim} is the simulation time, $\mathrm{CN_{av}}$ is the average coordination number of the respective shell and N_{ex} is the number of accounted exchange events. The most suitable value for t^* was resulted as 0.5 ps [45] corresponding to the mean lifetime of H-bonds in water [16].

The visualisation of the molecular movements stored in the trajectories completes the instrumentarium available for a very detailed and sophisticated analysis of the system's dynamics, including the mechanisms of ligand exchange, temporary distortions of complex species and formation of supramolecular structures.

3.3. Liquid water as crucial test case for the methods

As the analytical capabilities of QM/MM MD simulations exceed in many cases the limits of present experimental techniques and, therefore, supply data not yet confirmable by measurements, careful tests of the employed methodical framework are mandatory to assess the reliability of its predictions. In the case of QM/MM simulations, many experimentally accessible structural and thermodynamic data of solvated ions have been reproduced within the methodical limits [46,47], and in some cases, where the agreement was less favourable, the analysis of the simulations has provided strong hints that the model used for the interpretation of the measured data has to be refined (vide infra).

Liquid water represents the most suitable and crucial test case for the quality of the simulation framework, as a vast amount of experimental data is available, in particular most recent laser pulse spectroscopic data for the picosecond dynamics of this liquid [16] as well as combined X-ray and Raman investigations of its molecular structure [48]. Extensive QM/MM MD simulations for pure water have been performed, therefore, at various levels of theory, and the results of comparisons with experiment are very encouraging concerning the HF level of theory [49]. On the other hand, they confirmed the inadequacy of DFT methods, which predict a much too rigid geometry and by far too long MRT values [49]. Simulations at the MP/2 level of theory have indicated that the inclusion of electron correlation can still improve the results, but only if at least two coordination shells around a central water molecule are included in the QM region [49]. This extension to two shells could be realised so far only at HF level, but with very satisfactory results: A main structural unit, in which water dominantly forms two strong hydrogen bonds with an average lifetime of 0.35 ps was predicted. The same structural unit was found by the most recent experiments [48] and the average lifetime of a hydrogen bond in liquid water measured by femtosecond laser pulse spectroscopy was reported as 0.5 ps [16]. On the basis of these agreements, the data for solvated ions can be entrusted, especially, as in ion solvates much stronger binding occurs than in water, thus making the influence of correlation energy a minor factor [50,51]. The structural data obtained by the ab initio QM/MM MD simulations at different level of theory and the corresponding MRT values obtained for $t^* = 0$ (for determination of H-bond life time) and $t^* = 0.5$ (to obtain real exchange processes of neighbour molecules) are presented in Table 1. A video clip in the supplementary materials shows the dynamics of liquid water with its continuous H-bond forming and breaking.

Table 1
Maxima r_M of the O–O radial distribution function in Å, average coordination numbers CN and mean residence times τ in ps of pure water [49]

	r_{M1} [a]	r_{M1} [a]	$CN_{av,1}$ [b]	$CN_{av,2}$ [b]	$\tau^{0.5}_{D,1st}$ [c]	$\tau^{0.5}_{D,2nd}$ [c]
H_2O-1shell-HF	2.97	4.4	4.9	21.2	1.6	2.4
H_2O-1shell-MP2	2.87	4.7	4.7	22.8	2.5	2.4
H_2O-2shells-HF	2.92	–[d]	4.2	19.3	1.5	1.7

[a] First and second peak maximum of the O–O-RDF.
[b] First and second shell coordination number.
[c] First and second shell mean residence time; $t^* = 0.5$ ps.
[d] No distinct maximum oberservable.

4. Main group metal ions

Table 2 lists characteristic structural data, the average coordination numbers and the mean residence times of water ligands in the first and second hydration shell of several main group metal ions.

Most of these ions (except Mg(II), Pb(II) and the trivalent ions) exchange first shell ligands within the picosecond scale, some of them nearly as fast or even faster than coordination changes take place in pure water (K(I), Rb(I), Cs(I)). This phenomenon will be discussed separately in the section on 'structure breaking ions'. The second hydration shell is very labile in all cases, even the trivalent small Al(III) ion exchanges a ligand in this shell on average every 26 ps. A consequence of the rapid exchange rates are average coordination numbers composed of more than one species in all hydrates except those of the aforementioned ions with stable first coordination shell. The existence of differently coordinated hydrates within picoseconds, i.e. almost simultaneously, makes the structure very flexible and thus the reaction of these ions with other ligands extremely easy.

Most of the trends observed from lighter to heavier ions within the same group reflect the expected behaviour (increasing coordination number, decreasing stability of the hydrates). Sn(II) and Pb(II), however, show an unexpected increase of the ligand stability for the heavier ion, reflected in the MRT values [9]. A more detailed analysis of the dynamics of hydrated Pb(II) shows strong distortions, which occur in a concerted way involving only some of the ligands, and thus rarely pushing one of the first shell ligands into a position to leave this shell [51]. This ion, for which only very few experimental data are available, deserves further studies, therefore. The ion–ligand distances are basically in good agreement with experimental values from diffraction studies, as far as they are available [4,9]. The broadness of the first peaks in the corresponding RDFs and the rapid ligand exchange leading to varying coordination (cf. Fig. 2) numbers make clear, however, that these distances and the underlying structures can only be averaged values with a broad statistical deviation. The consequences of this for experimental studies will be discussed later.

Table 2
Maxima r_M of the Ion–O radial distribution functions in Å, average coordination numbers CN and mean residence times τ in ps of several main group metal ions

	r_{M1} [a]	r_{M2} [a]	$CN_{av,1}$ [b]	$CN_{av,2}$ [b]	$\tau^{0.5}_{D,1st}$ [c]	$\tau^{0.5}_{D,2nd}$ [c]	Reference
Li(I)	1.95	–	4.2	–	–	–	[52]
Na(I)	2.33	–	5.4	–	2.4	–	[53]
K(I)	2.81	–	8.3	–	2.0	–	[53]
Rb(I)	2.95	–	7.1	–	2.0	–	[54,85]
Cs(I)	3.25	–	7.8	–	1.5	–	[50]
Mg(II)	2.03	4.12	6.0	18.3	–	–	[55]
Ca(II)	2.46	4.78	7.6	19.1	42.6	4.4	[56,45]
Sr(II)	2.70	5.0	9.0	20.4	∼40	5.2	[54]
Ba(II)	2.86	5.0	9.3	23.5	5.5	1.7	[57]
Al(III)	1.86	4.73	6.0	12.2	–	26.4	[58,54]
Ga(III)	1.96	4.3	6.0	13.6	–	–	[54]
Sn(II)	2.51	4.9	8.0	23.7	9.0	3.5	[54]
Pb(II)	2.60	5.0	9.0	24.3	–	5.6	[51,54]

[a] First and second peak maximum of the Ion–O-RDF.
[b] First and second shell coordination number.
[c] First and second shell mean residence time; $t^* = 0.5$ ps.

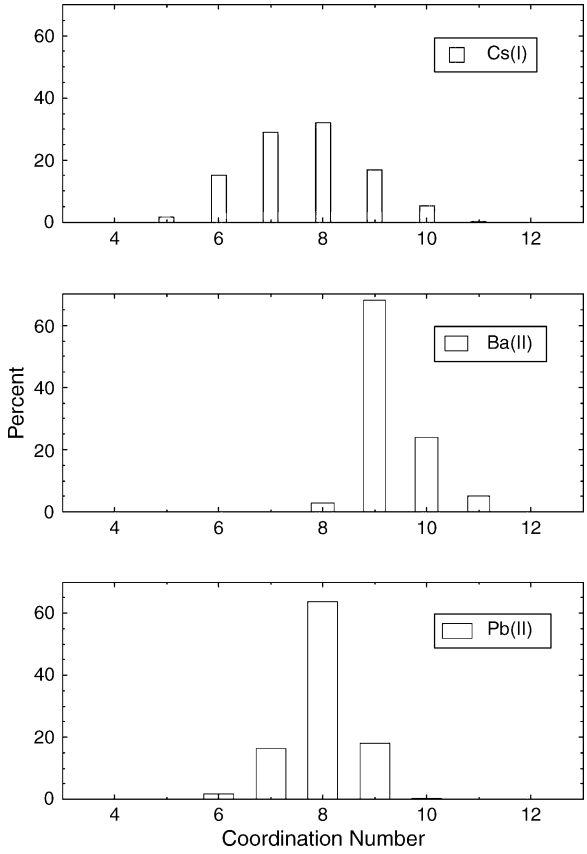

Fig. 2. First shell coordination number distributions obtained from QM/MM MD simulations of Cs(I), Ba(II) and Pb(II) in water.

5. First-row transition metal ions

5.1. General features

A number of di- and trivalent ions of this series have been studied by means of ab initio QM/MM MD simulations, and some of the results are collected in Table 3.

Table 3
Maxima r_M of the Ion–O radial distribution functions in Å, average coordination numbers CN and mean residence times τ in ps of several first-row transition metal ions

	r_{M1} [a]	r_{M2} [a]	$CN_{av,1}$ [b]	$CN_{av,2}$ [b]	$\tau^{0.5}_{d,2nd}$ [c]	Reference
V(II)	2.23	4.4	6.0	15.8	7.5	[32,45]
Mn(II)	2.25	4.4	6.0	15.9	6.8	[32,45]
Fe(II)	2.10	4.5	6.0	12.4	5.4	[59,45]
Co(II)	2.17	4.6	6.0	15.9	6.8	[60,45]
Ni(II)	2.12	4.5	6.0	13.7	6.3	[61,54]
Cu(II)	2.03/2.15/2.30	4.22	6.0	12.7	7.7	[62]
Zn(II)	2.15	4.5	6.0	14.7	10.5	[54]
Ti(III)	2.03/1.99/2.06/2.12/2.14	4.2	6.0	11.0	37	[63]
Cr(III)	1.92	4.4	6.0	15.4	7.5	[64,45]
Co(III)	1.97	4.3	6.0	15.2	11.0	[65,45]
Fe(III)	2.02	4.3	6.0	13.4	19.8	[59,45]

[a] First and second peak maximum of the Ion–O-RDF.
[b] First and second shell coordination number.
[c] Second shell mean residence time; $t^* = 0.5$ ps.

The collected data show at once a very characteristic common feature of all ions, namely the exclusive first-shell coordination of six ligands without observable exchange within the simulation time of 20–30 ps. Although the first shell coordination number remains constant, remarkable distortions of the octahedral hydrate structure occur frequently, even for trivalent ions such as Cr(III) with its very stable first shell [64]. Any theoretical treatment assuming a rigid first hydration shell [66] appears unjustified, therefore. The size of the second hydration shell varies between 13 and 16, indicating that the majority of these ligands are directly hydrogen-bonded to the first shell ligands. Mean residence times of second shell ligands are also quite similar, lying between 5 and 10 ps for divalent ions. For the triply charged ions, they vary over a wider scale. Generally, the transition metal ions can be considered as forming rather similar hydrates, with the exception of Cu(II) and Ti(III), for which the Jahn–Teller effect induces significant changes in structure and dynamics, thus deserving a separate discussion.

5.2. Jahn–Teller distorted ions

The geometrical distortions due to the dynamical Jahn Teller effect in solution are clearly reflected in the ligand distances of Cu(II) and Ti(III). It has been shown that this effect is of a very complex nature, with variations of the distortions occurring on the femtosecond scale and overlying picosecond phenomena [62,67], leading to a number of quite different structures visible from the splitted first RDF peaks as well as the associated vibrational spectra [62]. The Jahn–Teller effect is known to enhance the exchange rate of ligands by orders of magnitude compared to other transition metal ions [3] but for the hydrates it still lies beyond the range observable by the QM/MM simulations. Other ligands can change this, as will be seen later. Methodical investigations within the QM/MM formalism have shown that for the Jahn–Teller distorted ions the inclusion of two hydration shells is required for an accurate reproduction of experimental data, thus leading to a much higher computational effort [62]. This expansion of the QM region at Hartree–Fock level seems even more important than the inclusion of electron correlation, as demonstrated with the help of an MP/2-level simulation of hydrated Cu(II) [68]. Table 4 lists the results obtained at various levels of theory, and for the discussions in this section, the values obtained from the two-shell HF-level simulations have been considered as reference data.

The Jahn–Teller acceleration of the first shell exchange rate is not reflected in MRT values of the second shell, in contrary, second shell MRTs of Cu(II) and Ti(III) are the largest ones within the groups of di- and trivalent ions, respectively. At the same time, average second shell

Table 4
Maxima r_M of the Ion–O radial distribution functions in Å, average coordination numbers CN and mean residence times τ in ps of Jahn–Teller distorted transition metal ions

	r_{M1} [a]	r_{M2} [a]	$CN_{av,1}$ [b]	$CN_{av,2}$ [b]	$\tau^{0.5}_{D,2nd}$ [c]	Reference
Cu-1shell-HF	2.07/2.2	4.6	6.0	11.7	8	[67,45]
Cu-1shell-MP2	2.07/2.35/2.5	4.6	6.0	10.4	10	[68]
Cu-2shells-HF	2.03/2.15/2.3	4.2	6.0	12.7	3	[62]
Ti-1shell-HF	2.08/2.11/2.15	(4.7)	6.0	(8.0)	–	[63]
Ti-2shells-HF	2.03/1.99/2.06/ 2.12/2.14	4.2	6.0	11.0	37	[63]

[a] First and second peak maximum of the Ion–O-RDF.
[b] First and second shell coordination number.
[c] Second shell mean residence time; $t^* = 0.5$ ps.

coordination numbers of the Jahn–Teller distorted ions are smaller than for other comparable ions. The importance of geometrical distortions of complex geometries for the exchange dynamics, induced by the Jahn–Teller effect in combination with the binding of other ligands will be addressed further in Section 10.

6. Heavy metal ions

The definition of 'heavy metal' in chemistry is by far not so homogeneous as in the music genre of the same name. Mostly it refers to metals of high order number, belonging to the groups of second row transition metals, lanthanides/actinides or to the 5th and 6th period of main group metals. Mostly they do not have any biological relevance, but rather display toxic effects in living organisms, which in a few cases can be used for therapeutic pharmacological purposes [69]. From the viewpoint of quantum chemistry, they are characterised by the importance of relativistic effects, which in all ab initio QM/MM simulations have been taken into account by the use of relativistically corrected effective core potentials (ECP) in combination with ECP-optimised basis sets [70]. Table 5 lists the characteristic data of the examples studied, and although far from any completeness, the comparison of these data allows a few conclusions about specific properties being displayed by such 'heavy metal' ions in water.

Common characteristics are the rather labile first hydration shell, reflected in wider coordination number distributions (examples in Fig. 1) and short ligand life times in this shell, beyond measurability with present experimental techniques. Second shell MRTs are extremely short, underlining the rapid structural changes in the surroundings of these ions in solution. Exceptions from this rule are only Cd(II) – being the lightest example among the investigated ions – and Pb(II), which has been discussed already in Section 4 as being a particular case.

The extremely fast ligand exchange rates in first and second shell of Cs(I) cause a strong 'structure-breaking' effect, which will be discussed in Section 8. Au(I) also belongs to the 'structure-breaking' ions, but for somewhat different reasons. Ag(I) is characterised by fast changes between 3 and 6 ligands in the first shell [71], and the easy removal of first shell ligands upon binding of other ligands, which in the case of Au(I) can even lead to a complete removal of the first hydration shell (vide infra, Section 10). The comparison of Ba(II) and Pb(II) demonstrates the strong influence of the inner electrons and of electrons remaining in the valence shell of an ion within the same period on the stability of a hydration shell: second shell ligands of Pb(II) exchange at the same rate as first shell ligands of Ba(II), and the first shell of Pb(II) is much more stable than that of other metal ions of comparable atomic number in the investigated series. La(III)–water exchange rates have apparently been underestimated in the past. Although the sampling of such processes in the simulations performed to date is still very poor, it can be estimated that the MRT of water in the immediate surrounding of La(III) is clearly below the nanosecond range expected [10] (Table 5).

7. Labile solvates

'Labile' solvates can be used as a term for all solvated ions, whose ligand exchange occurs at rates of $\geq 10^{10}$, thus creating an almost simultaneous presence of several solvate species with different coordination numbers and hence structures. This behaviour evidently has consequences for any model attempting to describe reaction mechanisms of the ion in solution, and on the interpretation of any spectroscopic data obtained from solutions of such ions. According to this definition and the data collected in Tables 2, 3 and 5, all alkali ions, all alkaline earth metal ions above Mg(II), and most of the 'heavy metal' ions have to be termed 'labile' (c.f. Table 6). Within this group, however, one observes still major differences of lability, as the comparison of Na(I) and K(I) illustrates quite well, with its transition from 'structure-forming' to 'structure-breaking' properties (video clip in supplementary materials). The degree of lability of a hydration shell is not only an important factor determining the reactivity of ions in solution via the speed of any ligand exchange, it

Table 5
Maxima r_M of the Ion–O radial distribution functions in Å, average coordination numbers CN and mean residence times τ in ps of several heavy metal ions

	r_{M1} [a]	r_{M2} [a]	$CN_{av,1}$ [b]	$CN_{av,2}$ [b]	$\tau^{0.5}_{D,1st}$ [c]	$\tau^{0.5}_{D,2nd}$ [c]	Reference
Cs(I)	3.25	5.2	7.8	20	1.5	1.3	[50]
Ag(I)	2.6	4.6	5.4	17.8	5.5	2.6	[71,45]
Au(I)	2.45	4.9	4.7	33	3.1	4.6	[72,45]
Ba(II)	2.86	5.0	9.3	23.5	5.5	1.7	[57]
Pb(II)	2.60	5.0	9.0	24.3	–	5.6	[51,54]
Cd(II)	2.33	4.8	6.0	11.7	–	4.6	[73,45]
Hg(II)	2.42	4.6	6.2	21.7	23.6	4.8	[69,45]
La(III)	2.67	4.9	9.2	∼90	23.2	7.4	[54]

[a] First and second peak maximum of the Ion–O-RDF.
[b] First and second shell coordination number.
[c] First and Second shell mean residence time; $t^* = 0.5$ ps.

Table 6
Maxima r_M of the Ion–O radial distribution functions in Å, average coordination numbers CN and mean residence times τ in ps of several labile ions

	r_{M1} [a]	r_{M2} [a]	$CN_{av,1}$ [b]	$CN_{av,2}$ [b]	$\tau^{0.5}_{D,1st}$ [c]	$\tau^{0.5}_{D,2nd}$ [c]	Reference
Ag(I)	2.6	4.6	5.4	17.8	5.5	2.6	[71,45]
Au(I)	2.45	4.9	4.7	33	3.1	4.6	[72,45]
Ca(II)	2.46	4.78	7.6	19.1	42.6	4.4	[56,45]
Sr(II)	2.70	5.0	9.0	20.4	∼40	5.2	[54]
Ba(II)	2.86	5.0	9.3	23.5	5.5	1.7	[57]
Hg(II)	2.42	4.6	6.2	21.7	23.6	4.8	[69,45]

[a] First and second peak maximum of the Ion–O-RDF.
[b] First and second shell coordination number.
[c] First and second shell mean residence time; $t^* = 0.5$ ps.

also determines the ability of ions to abandon their hydration shell in order to enter specific channels for these ions in membranes [53]. Thus, a number of biological processes are directly or indirectly related to the ultrafast dynamics of ions in aqueous environment, which have only become accessible through the accuracy of ab initio QM/MM simulations.

The fact that a large number of the hydrated ions belongs to the class of 'labile' solvates has doubtlessly to be considered in the interpretation (or re-interpretation) of spectroscopic data in the course of structural investigations of such ions in solution and in the discussion of ligand exchange mechanism reaction mechanisms. The fitting of X-ray or neutron diffraction data would have to take into account the fact that a mixture of species with different coordination and structure is present, and that fitting to a single model structure can be a serious source of error for the determination of 'real' bond lengths and angles. At the same time, models for reaction mechanisms, which are usually classified as 'associative', 'dissociative' and 'interchange' [10], appear too simplistic for the complicated dynamics of solvated ions. Therefore, also in this case a re-interpretation of measurable quantities such as the activation volume of ligand exchange reactions[10] appears desirable. The visualisation of the trajectories of sufficiently accurate simulations is a helpful tool not only for the illustration of the exchange dynamics, but – in combination with ion–ligand distance plots as exemplified in Fig. 3 – also an instrument to classify reaction mechanisms in a more detailed way. Therefore, a specific visualisation tool for such trajectories has been developed recently [74], which has been utilised for the production of the video clips supplied as supporting material for this paper and for several other data evaluations such as MRT values.

8. Structure breaking ions

Among the 'labile' ions discussed in the previous section, some exhibit a specific property, which has been termed 'structure-breaking' several decades ago on the basis of NMR measurements [75], showing that relaxation times of water molecules near these ions are shorter than in the pure solvent. Cs(I) is the most 'prominent' example for this property, which is usually explained by the large space occupied in the solvent by such ions, in connection with a weak ligand binding. The investigation of hydrated ions by means of ab initio QM/MM MD simulations basically supports this characterisation, but supplies a much more differentiated picture of the 'structure-breaking' effect.

Within the series of alkali metal ions, Li(I) and Na(I) still display a rather well-ordered structure of their hydration shell. K(I), however, looses first-shell ligands quite frequently, thus repeatedly remaining in lower coordination state for some time and not displaying any specific geometrical order of this shell. Together with its extremely short MRT

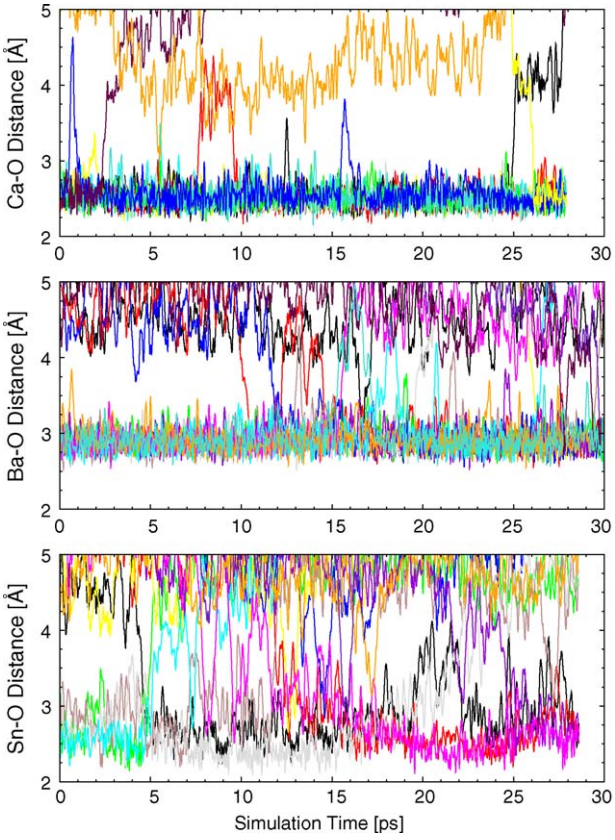

Fig. 3. Distance plots of water molecules showing water exchange processes within the time scale of the QM/MM MD simulation.

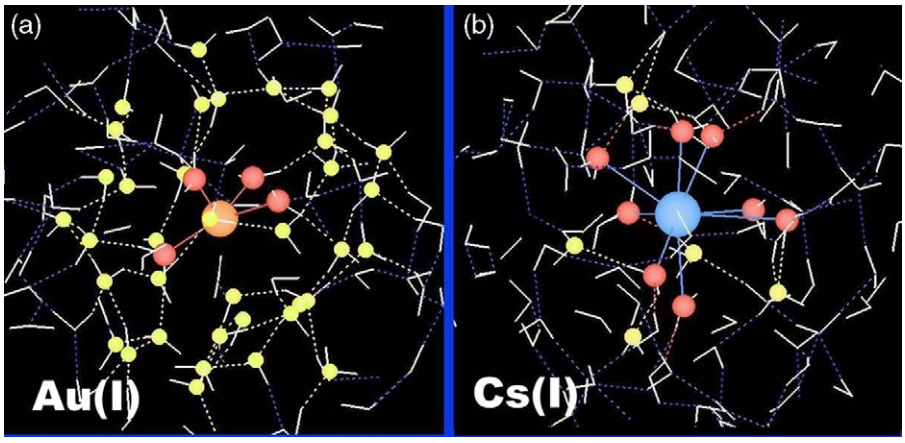

Fig. 4. Snapshots of the QM/MM MD simulations of hydrated Au(I) and Cs(I).

value the over-all effect is a strong perturbation of the solvent structure without formation of any new order. This effect becomes more pronounced for Rb(I) and Cs(I), where due to the weaker ligand binding smaller average coordination numbers result. Any estimated second shell coordination numbers for alkali ions except Li(I) are rather an indication of the number of bulk molecules affected by the presence of the hydrated ion than of a real structural entity. A common feature of the 'structure breakers' K(I)–Cs(I) seems a first shell coordination number of 7–8 and first shell MRT values similar or below that of pure water, corresponding to the experimentally observed reduced relaxation times [9].

Inspection of the solvation structure and dynamics of the other ions studied here reveals yet another possible type of 'structure-breaking' effect, exemplified by hydrated Au(I). This ion has a much lower ($\leq$5) average first-shell coordination number, but an excessively large second hydration shell ($\geq$30), which is more tightly bound than the same shell in the case of the heavier alkali metal ions. The exchange between first and second shell ligands is even faster than that between second shell and bulk, thus stabilising a very large entity in the solution structure. Fig. 4a and b shows snapshot pictures of the different structures of Cs(I) and Au(I) responsible for both types of the 'structure-breaking' effect, and the video clips in the supporting materials illustrate the different dynamical behaviour of these two ions.

Finally, it should be mentioned that some other ions can produce a similar 'structure-breaking' effect, at least concerning the reorientational speed of solvent molecules, due to their rapid second shell/bulk exchange rates, reflected in very short MRT values of the second shell. Their second shell is stable and distinct enough to create a larger spatial entity within the solvent structure, but at the same time exchange of ligands in this shell is so fast that perturbing effects will be realised in its environment. Ba(II) and Ag(I) can serve as examples for this effect. In Table 7, the properties of the 'structure breakers' have been collected for a better comparability.

Table 7
Maxima r_M of the Ion–O radial distribution functions in Å, average coordination numbers CN and mean residence times τ in ps of 'structure breaking' ions

	r_{M1} [a]	r_{M2} [a]	$CN_{av,1}$ [b]	$CN_{av,2}$ [b]	$\tau^{0.5}_{D,1st}$ [c]	$\tau^{0.5}_{D,2nd}$ [c]	Reference
K(I)	2.81	–	8.3	–	2.0	–	[53]
Rb(I)	2.95	–	7.1	–	2.0	–	[54,85]
Cs(I)	3.25	–	7.8	–	1.5	–	[50]
Ba(II)	2.86	5.0	9.3	23.5	5.5	1.7	[57]
Ag(I)	2.6	4.6	5.4	17.8	5.5	2.6	[71,45]
Au(I)	2.45	4.9	4.7	33	3.1	4.6	[72,45]

[a] First and second peak maximum of the Ion–O-RDF.
[b] First and second shell coordination number.
[c] First and second shell mean residence time; $t^* = 0.5$ ps.

9. Ions in liquid ammonia

In order to obtain some information about similarities and differences of ion coordination and dynamics upon change of the solvent, a few ions have been investigated by ab initio QM/MM MD simulations with liquid ammonia as solvent. The main data from these simulations are collected in Table 8. For the first-row transition metal ions, an octahedral arrangement with six ligands is observed as in the case of water, with M(II)–ligand distances slightly

Table 8
Maxima r_M of the Ion–N radial distribution functions in Å, average coordination numbers CN and mean residence times τ in ps in pure ammonia solution

	r_{M1} [a]	r_{M2} [a]	$CN_{av,1}$ [b]	$CN_{av,2}$ [b]	$\tau^{0.5}_{D,1st}$ [c]	$\tau^{0.5}_{D,2nd}$ [c]	Reference
Co^{2+}	2.22	4.8	6.0	16.6	–	28	[76]
Ni^{2+}	2.17	4.9	6.0	23.6	–	3.0	[54]
Cu^{2+}	2.05/2.17	4.9	5.98	23.5	32	3.2	[77]
Ag^{+}	2.54	5.0	4.0	26	–	13	[78]
Au^{+}	2.15	5.0	2	27	–	7.1	[79]

[a] First and second peak maximum of the Ion–N-RDF.
[b] First and second shell coordination number.
[c] First and second shell mean residence time; $t^* = 0.5$ ps.

higher than in water. Quite striking is the difference in the ligand exchange rate of the remarkably Jahn–Teller distorted Cu(II)–ammonia complex, where the mean residence time of a first-shell ligand is now situated in the picosecond range. In the second shell, both Cu(II) and Ni(II) exchange ligands very rapidly, whereas Co(II) retains the ligands about 10 times longer in its relatively smaller second shell.

Silver ion clearly shows a higher affinity to ammonia than to water, forming a very stable first shell with four ligands and a large second shell with a much larger MRT value than in water (double the value of first shell ligands in water!). The behaviour of Au(I) is very similar, but in this case the stable inner complex is formed with only two ammonia molecules in a fairly linear N. . .Au. . .N arrangement. The second shell is very large, with ligands exchanging again slower than their analogues in water.

From these few examples, general principles cannot be concluded. It seems, however, that the differences are mainly determined by the individual binding strength of the ammonia molecules to the ions compared to water (or, more generally, the ion–N versus the ion–O bond strength), but that steric factors and particular stabilisations of lower-coordinated species can provoke surprising changes in the solvation of metal ions. In the light of these findings it appeared of particular interest to investigate the influence of heteroligands (i.e. other ligands than water) in aqueous solution and the behaviour of ions in mixed solvents.

10. Ions with different ligands and ions in mixed solvents

Exchange of water ligands by heteroligands and/or the competition of different ligands in binding to an ion are not only the basis for the frequently observed and occasionally practically applied phenomenon of preferential solvation, they also serve as a useful model for the reactivity of metal ion complexes with different coordination sites, e.g. O and N binding sites. For such model systems, ab initio QM/MM MD simulations are again a quite powerful tool to study changes in coordination, structure and dynamics induced by such heteroligands. Two different approaches have been taken to describe these effects. In the first one, ammonia ligands known to form a very stable bond to some transition metal ions have been attached to these ions in increasing number, studying the exchange of water ligands in the modified solvation shells. The main results of these studies are summarised in Table 9. In the case of the Jahn–Teller distorted ion Cu(II) with its faster exchange rate in comparison to other divalent transition metal ions, the effect of the heteroligand becomes visible already after the binding of just one such ligand: The mean residence time for the remaining five water ligands is reduced by at least one order of magnitude, from the estimated 1 ns for the hexahydrate to a value slightly above 100 ps. Binding of a second NH_3 ligand enhances this effect by a factor of 1.5–3.3, depending on whether the second ligand is located in *cis* or *trans* position to the first one. In the case of the Ni(II) hydrate with its much slower exchange rate, this shift of mean residence times into the picosecond range observable by the simulations becomes visible only after the binding of three NH_3 ligands, reaching 27 and 16 ps for the triammine and tetrammine complexes, respectively.

These results have some important implications for the reaction dynamics of such ions in biological complexes. The binding of the metal ion to nitrogen binding sites apparently facilitates a rapid exchange of water (and possibly other O-coordinated ligands), thus allowing important enzymatic reactions to proceed at a faster pace. This indication certainly deserves further studies with a variety of other ligands mimicking the binding sites in biologically relevant metal complexes.

In the second approach, simulations were performed for ions in 18.5% aqueous ammonia solution, in order to observe preferential solvation phenomena and the formation of equilibrium species with mixed ligands. Table 10 summarises some of the results of these investigations.

In the case of the main group metal ions Li(I), Na(I), Mg(II) and Ca(II) various complex species with different

Table 9
Maxima r_M of the Ion–O radial distribution functions in Å, average coordination numbers CN and mean residence times τ in ps of several amine complexes transition metal ions

	r_{M1} [a]	r_{M2} [a]	$CN_{av,1}$ [b]	$CN_{av,2}$ [b]	$\tau^{0.5}_{D,1st}$ [c]	$\tau^{0.5}_{D,2nd}$ [c]	Reference
Cu–1NH_3	2.13	4.6	5.1	12.9	115	21	[12]
Cu–2NH_3(*cis*)	2.13(3.12)	4.6	4.4	14.0	75	21	[12]
Cu–2NH_3(*trans*)	2.28(3.07)	4.8	4.6	14.1	35	20	[12]
Ni–1NH_3	2.12	4.5	5.0	19.3	–	7.1	[54,86]
Ni–2NH_3(*cis*)	2.17	4.6	3.9	26.4	–	7.0	[54,86]
Ni–2NH_3(*trans*)	2.18	4.6	4.0	24.3	–	7.8	[54,86]
Ni–3NH_3	2.27	4.7	2.9	28.0	27	5.6	[54,86]
Ni–4NH_3	2.22	4.2	1.9	34.0	16	10	[54,86]

[a] First and second peak maximum of the Ion–O-RDF.
[b] First and second shell coordination number.
[c] First and second shell mean residence time; $t^* = 0.5$ ps.

Table 10
Maxima r_M of the Ion–O and Ion–N radial distribution functions in Å, average coordination numbers CN and mean residence times τ in ps of cations in mixed electrolyte solutions

	r_{1H_2O}[a]	r_{2H_2O}[a]	CN_{1H_2O}[c]	CN_{2H_2O}[c]	r_{1NH_3}[b]	r_{2NH_3}[b]	CN_{1NH_3}[c]	CN_{2NH_3}[c]	Reference
Li^+	1.94	–	3.1	–	2.08	–	1.0	–	[80]
Na^+	2.30	–	3.7	–	2.41	–	1.8	–	[81]
Mg^{2+}	2.16	4.07	5.0	15.3	2.16	4.13	1.0	5.7	[82]
Ca^{2+}	2.44	4.53	5.2	19.7	2.64	4.54	2.0	4.9	[83]
Ag^+	2.4	–	2.0	–	2.7	–	3.8	–	[54]
Au^+	–	3.9	–	26.1	2.13	5.9	2.0	5.3	[54]

[a] First and second peak maximum of the Ion–O-RDF.
[b] First and second peak maximum of the Ion–N-RDF.
[c] First and second shell water and ammonia coordination number.

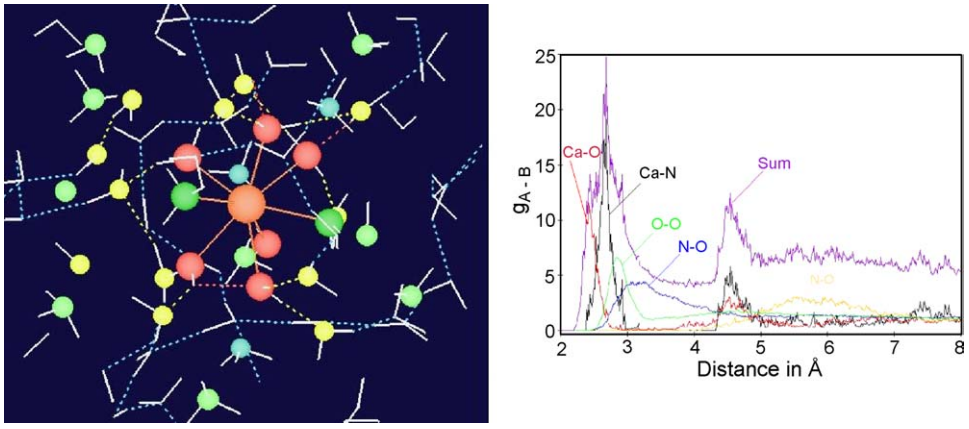

Fig. 5. Snapshot of the QM/MM MD simulations of Ca(II) in mixed electrolyte solution (left picture) and all corresponding RDFs (right picture).

coordination and thus structure are interchanging within the picosecond range [80–83], whereas Ag(I) and Au(I) both form very stable diammine complexes associated with a rather labile outer hydration sphere [54].

The preference for either water or ammonia ligands is in fair agreement with the concept of 'hard' and 'soft' Lewis acids, preferring bases of the same quality: the 'harder' Li(I) and Mg(II) bind ammonia ligands (N/O ratio of 0.25 and 0.20, respectively) much less, compared to the 'softer' Na(I) and Ca(II) with N/O ratio of 0.49 and 0.44, respectively, which is clearly above the statistical ratio of the 18.5% aqueous ammonia solution and hence a good example for a preferential solvation phenomenon.

Ag(I) demonstrates this phenomenon even much more by a ratio of 1.9 in favour of ammonia ligands, and Au(I) finally does not bind water molecules directly but uses them only to solvate its diammine complex at larger distances with a second shell.

The fractional coordination numbers for the solvate compositions prove that a number of different species contribute to these average values. The coordination number distribution plots for these ions in aqueous ammonia in the references [80–82] illustrate that the number of these species is large, and thus numerous simultaneously present solvate structures make the solution a very complex system. Any detailed experimental analysis of such systems without the help of theoretical instruments appears rather impossible, therefore. A simple diagram of the RDFs of atom–atom pairs, which contain the averaged distances encountered – and thus measured by diffraction methods – for Ca(II) in aqueous ammonia (Fig. 5) immediately shows the ambiguity of a not-resolved overlay of all these curves, and this averaged diagram does not yet take into account all the dynamical effects, leading to continuously changing coordinations, compositions and structures of species (video clip in supporting materials).

11. Conclusions for future theoretical and experimental work

The list of simulations of solvated metal ions presented here – although representing a total amount of about 25 years of computing time – is at the best an exemplifying selection of a large amount of investigations worthwhile to be undertaken in the future by the tools ab initio QM/MM simulations provide for the study of ions' reactivity and behaviour in solution, and further in complex chemistry and biochemistry. The general perspectives for the future work are quite

favourable, however, considering Moore's law that available computing speed and capacity doubles every 12–18 months, while its price is constantly decreasing. In addition, methodical developments in quantum chemical calculation methods show some promising signs indicating more rapid algorithms to become available [84]. This development will soon allow further methodical improvements to be implemented in the QM/MM MD formalism, in particular a routinely included second solvation shell, but also the upgrade to correlated ab initio levels of theory such as MP/2 or higher, and the usage of larger basis sets. Improvements in DFT functionals (B3PW91 [27] is a promising step) may open this track for an alternative access to studies of solvated ions and their complexes.

The examples presented in this paper, in particular those for the rapid exchange dynamics and the thus resulting multi-species distributions in solution strongly suggest a closer co-operation between experimental and theoretical investigators in all studies related to structure and dynamics of solvated ions. This refers to the selection of appropriate models for the fitting of spectroscopic data as well as to the determination of ligand exchange mechanisms and associated rate constants. In the latter case, theoretical investigations may still be the only instrument to obtain reliable data for ultrafast reactions below the nanosecond range, but it is hoped that the development of laser pulse spectroscopy leading to its application to solvated ions could catch up to close this gap in the near future.

The important field of more concentrated solutions, where a number of cations and anions are present, is still not within the reach of ab initio QM/MM simulations and will remain, therefore, a domain of classical simulations and experimental work for quite some time to come. The results for single ions and their complexes accessible by the QM/MM formalism should prove helpful, however, to develop better potential functions for the classical simulations, thus supporting progress in this field as well.

Appendix A. Supplementary data

Supplementary data associated with this paper can be found, in the online version, at doi:10.1016/j.ccr.2005.03.032.

References

[1] D.T. Richens, The Chemistry of Aqua Ions: Synthesis, Structure and Reactivity: A Tour Through the Periodic Table of the Elements, 1st ed., Wiley, New York, 1997.
[2] S.F. Lincoln, A. Merbach, in: Advances in Inorganic Chemistry, vol. 42, Academic Press, 1995, p. 1.
[3] D.H. Powell, L. Helm, A.E. Merbach, J. Chem. Phys. 95 (12) (1991) 9258.
[4] G.W. Neilson, A.K. Adya, Ann. Rep. Chem. Sect. C 93 (1996) 101.
[5] R. Åkesson, L.G.M. Pettersson, M. Sandström, U. Wahlgren, J. Phys. Chem. 96 (1) (1992) 150.
[6] R. Åkesson, L.G.M. Pettersson, M. Sandström, P.E.M. Siegbahn, U. Wahlgren, J. Phys. Chem. 97 (15) (1993) 3765.
[7] R. Åkesson, L.G.M. Pettersson, M. Sandström, U. Wahlgren, J. Am. Chem. Soc. 116 (19) (1994) 8705.
[8] R. Åkesson, L.G.M. Pettersson, M. Sandström, U. Wahlgren, J. Am. Chem. Soc. 116 (19) (1994) 8691.
[9] H. Ohtaki, T. Radnai, Chem. Rev. 93 (3) (1993) 1157.
[10] L. Helm, A.E. Merbach, Coord. Chem. Rev. 187 (1999) 151.
[11] B.M. Rode, C.F. Schwenk, A. Tongraar, J. Mol. Liq. 110 (2004) 105.
[12] C.F. Schwenk, B.M. Rode, Phys. Chem. Chem. Phys. 5 (2003) 3418.
[13] C.F. Schwenk, B.M. Rode, Chem. Commun. (2003) 1286.
[14] A.G. Desai, H.W. Dodgen, J.P. Hunt, J. Am. Chem. Soc. 91 (1969) 5001.
[15] I. Nagypál, F. Debreczeni, Inorg. Chim. Acta 81 (1984) 69.
[16] A.J. Lock, S. Woutersen, H.J. Bakker, Femtochemistry and Femtobiology, World Scientific, 2001.
[17] M.J. Elrod, R.J. Saykally, Chem. Rev. 94 (7) (1994) 1975.
[18] E. Clementi, H. Kistenmacher, W. Kolos, S. Romano, Theor. Chim. Acta 55 (1980) 257.
[19] L.A. Curtiss, R. Jurgens, J. Phys. Chem. 94 (14) (1990) 5509.
[20] F. Floris, M. Persico, A. Tani, J. Tomasi, Chem. Phys. 195 (1995) 207.
[21] R.R. Pappalardo, E.S. Marcos, J. Phys. Chem. 97 (17) (1993) 4500.
[22] J.M. Martínez, R.R. Pappalardo, E.S. Marcos, J. Am. Chem. Soc. 121 (13) (1999) 3175.
[23] T. Kerdcharoen, K.R. Liedl, B.M. Rode, Chem. Phys. 211 (1996) 313.
[24] R. Car, M. Parinello, Phys. Rev. Lett. 55 (22) (1985) 2471.
[25] A. Pasquarello, I. Petri, P.S. Salmon, O. Parisel, R. Car, É. Tóth, D.H. Powell, H.E. Fischer, L. Helm, A. Merbach, Science 291 (2001) 856.
[26] I. Bakó, J. Hutter, G. Pálinkás, J. Chem. Phys. 117 (21) (2002) 9838.
[27] F. Jensen, Introduction to Computational Chemistry, Wiley, 1999.
[28] A. Warshel, M. Levitt, J. Mol. Biol. 103 (1976) 227.
[29] M.J. Field, P.A. Bash, M. Karplus, J. Comput. Chem. 11 (6) (1990) 700.
[30] J. Gao, in: K.B. Lipkowitz, D.B. Boyd (Eds.), Reviews in Computational Chemistry, vol. 7, VCH Publishers, New York, 1996, chapter 3, p. 119.
[31] D. Bakowies, W. Thiel, J. Phys. Chem. 100 (25) (1996) 10580.
[32] C.F. Schwenk, H.H. Loeffler, B.M. Rode, J. Am. Chem. Soc. 125 (2003) 1618.
[33] R. Ahlrichs, M. Bär, M. Häser, H. Horn, C. Kölmel, Chem. Phys. Lett. 162 (3) (1989) 165.
[34] S. Brode, H. Horn, M. Ehrig, D. Moldrup, J.E. Rice, R. Ahlrichs, J. Comput. Chem. 14 (10) (1993) 1142.
[35] R. Ahlrichs, M. von Arnim, in: E. Clementi, G. Corongiu (Eds.), Methods and Techniques in Computational Chemistry: METECC-95, STEF, Cagliari, 1995, chapter 13, p. 5.
[36] M. von Arnim, R. Ahlrichs, J. Comput. Chem. 19 (15) (1998) 1746.
[37] H.J.C. Berendsen, J.P.M. Postma, W.F. van Gunsteren, A. DiNola, J.R. Haak, J. Phys. Chem. 81 (1984) 3684.
[38] F.H. Stillinger, A. Rahman, J. Chem. Phys. 68 (2) (1978) 666.
[39] P. Bopp, G. Janscó, K. Heinzinger, Chem. Phys. Lett. 98 (2) (1983) 129.
[40] H.L. Lemberg, F.H. Stillinger, J. Chem. Phys. 62 (5) (1975) 1677.
[41] K. Kuchitsu, Y. Morino, Bull. Chem. Soc. Jpn. 38 (1965) 814.
[42] P. Bopp, Chem. Phys. 106 (1986) 205.
[43] E. Spohr, G. Pálinkás, K. Heinzinger, P. Bopp, M.M. Probst, J. Phys. Chem. 92 (23) (1988) 6754.
[44] C.F. Schwenk, M.J. Loferer, B.M. Rode, Chem. Phys. Lett. 382 (2003) 460.
[45] T.S. Hofer, H.T. Tran, C.F. Schwenk, B.M. Rode, J. Comput. Chem. 25 (2004) 211.
[46] Y. Marcus, J. Chem. Soc., Faraday Trans. 87 (17) (1991) 2995.
[47] M.C. Day, J. Selbin, Theoretical Inorganic Chemistry, Reinhold Publisher Cooperation, New York, 1962.

[48] P. Wernet, D. Nordlund, U. Bergmann, M. Cavalleri, M. Odelius, H. Ogasawara, Å. Näslund, T.K. Hirsch, L. Ojamäe, P. Glatzel, L.G.M. Petterson, A. Nilsson, Science 304 (2004) 995.
[49] D. Xenides, B.R. Randolf, B.M. Rode, J. Chem. Phys. (2005).
[50] C.F. Schwenk, T.S. Hofer, B.M. Rode, J. Phys. Chem. A 108 (2004) 1509.
[51] T.S. Hofer, B.M. Rode, J. Phys. Chem. 121 (2004) 6406.
[52] H.H. Loeffler, B.M. Rode, J. Chem. Phys. 117 (1) (2002) 110.
[53] A. Tongraar, K.R. Liedl, B.M. Rode, J. Phys. Chem. A 102 (50) (1998) 10340.
[54] B.M. Rode, C.F. Schwenk, T. Hofer, D. Xenides, R. Armunanto, C. Kritayakornupong, unpublished results.
[55] A. Tongraar, B.M. Rode, Chem. Phys. Lett. 346 (2001) 485.
[56] C.F. Schwenk, H.H. Loeffler, B.M. Rode, J. Chem. Phys. 115 (23) (2001) 10808.
[57] T.S. Hofer, B.M. Rode, B.R. Randolf, Chem. Phys. 312 (2005) 81–88.
[58] T.S. Hofer, B.M. Rode, B.R. Randolf, Phys. Chem. Chem. Phys. 7 (2005) 1382–1387.
[59] T. Remsungnen, B.M. Rode, J. Phys. Chem. A 107 (2003) 2324.
[60] R. Armunanto, C.F. Schwenk, B.M. Rode, Chem. Phys. 295 (2003) 63.
[61] Y. Inada, A.M. Mohammed, H.H. Loeffler, B.M. Rode, J. Phys. Chem. A 106 (29) (2002) 6783.
[62] C.F. Schwenk, B.M. Rode, J. Chem. Phys. 119 (18) (2003) 9523.
[63] C. Kritayakornupong, K. Plankensteiner, B.M. Rode, Chem. Phys. Chem. 5 (2004) 1499.
[64] C. Kritayakornupong, K. Plankensteiner, B.M. Rode, J. Comput. Chem. 25 (2004) 1576.
[65] C. Kritayakornupong, K. Plankensteiner, B.M. Rode, J. Phys. Chem. 119 (12) (2003) 6068.
[66] A. Bleuzen, F. Foglia, E. Furet, L. Helm, A.E. Merbach, J. Weber, J. Am. Chem. Soc. 118 (50) (1996) 12777.
[67] C.F. Schwenk, B.M. Rode, Chem. Phys. Chem. 4 (9) (2003) 931.
[68] C.F. Schwenk, B.M. Rode, J. Am. Chem. Soc. 126 (2004) 12786.
[69] C. Kritayakornupong, B.M. Rode, J. Chem. Phys. 118 (2003) 5065.
[70] P.J. Hay, W.R. Wadt, J. Chem. Phys. 82 (1) (1985) 270.
[71] R. Armunanto, C.F. Schwenk, B.M. Rode, J. Phys. Chem. A 107 (17) (2003) 3132.
[72] R. Armunanto, C.F. Schwenk, H.T. Tran, B.M. Rode, J. Am. Chem. Soc. 126 (2004) 2582.
[73] C. Kritayakornupong, K. Plankensteiner, B.M. Rode, J. Phys. Chem. A 107 (2003) 10330.
[74] H.T. Tran, B.M. Rode, http://www.molvision.com, 2002.
[75] H.G. Hertz, Water: A Comprehensive Treatise, vol. 3, Plenum Press, New York, 1973.
[76] R. Armunanto, C.F. Schwenk, B.R. Randolf, B.M. Rode, Chem. Phys. 305 (2004) 135.
[77] C.F. Schwenk, B.M. Rode, Chem. Phys. Chem. 5 (2004) 342.
[78] R. Armunanto, C.F. Schwenk, B.R. Randolf, B.M. Rode, Chem. Phys. Lett. 388 (2004) 395.
[79] R. Armunanto, C.F. Schwenk, B.M. Rode, J. Am. Chem. Soc. 126 (2004) 9934.
[80] A. Tongraar, B.M. Rode, J. Phys. Chem. A 103 (42) (1999) 8524.
[81] A. Tongraar, B.M. Rode, J. Phys. Chem. A 105 (2) (2001) 506.
[82] A. Tongraar, K. Sagarik, B.M. Rode, J. Phys. Chem. B 105 (54) (2001) 10559.
[83] A. Tongraar, K. Sagarik, B.M. Rode, Phys. Chem. Chem. Phys. 4 (2002) 628.
[84] D.A. Mazziotti, J. Chem. Phys. 115 (2001) 8305.
[85] T.S. Hofer B.M. Rode, B.R. Randolf, J. Comput. Chem. 26 (2005) 949.
[86] C.F. Schwenk, T.S. Hofer, B.R. Randolf, B.M. Rode, Phys. Chem. Chem. Phys. 7 (2005) 1669.